HHS Public Access

Author manuscript

Neuroimage. Author manuscript; available in PMC 2018 June 01.

Published in final edited form as:

Neuroimage. 2018 June ; 173: 165–175. doi:10.1016/j.neuroimage.2018.02.028.

Effects of resting state condition on reliability, trait specificity, and network connectivity of brain function measured with arterial spin labeled perfusion MRI

Zhengjun Li[a,1], **Marta Vidorreta**[b,1], **Natalie Katchmar**[c], **David C. Alsop**[d], **Daniel H. Wolf**[c], and **John A. Detre**[a,b,*]

[a]Department of Neurology, University of Pennsylvania Perelman School of Medicine, USA

[b]Department of Radiology, University of Pennsylvania Perelman School of Medicine, USA

[c]Department of Psychiatry, University of Pennsylvania Perelman School of Medicine, USA

[d]Department of Radiology, Beth Israel Deaconess Medical Center, USA

Abstract

Resting state fMRI (rs-fMRI) provides imaging biomarkers of task-independent brain function that can be associated with clinical variables or modulated by interventions such as behavioral training or pharmacological manipulations. These biomarkers include time-averaged regional brain function as manifested by regional cerebral blood flow (CBF) measured using arterial spin labeled (ASL) perfusion MRI and correlated temporal fluctuations of function across brain networks with either ASL or blood oxygenation level dependent (BOLD) fMRI. Resting-state studies are typically carried out using just one of several prescribed state conditions such as eyes closed (EC), eyes open (EO), or visual fixation on a cross-hair (FIX), which may affect the reliability and specificity of rs-fMRI. In this study, we collected test-retest ASL MRI data during 4 resting-state task conditions: EC, EO, FIX and PVT (low-frequency psychomotor vigilance task), and examined the effects of these task conditions on reliability and reproducibility as well as trait specificity of regional brain function. We also acquired resting-state BOLD fMRI under FIX and compared the network connectivity reliabilities between the four ASL conditions and the BOLD FIX condition. For resting-state ASL data, EC provided the highest CBF reliability, reproducibility, trait specificity, and network connectivity reliability, followed by EO, while FIX was lowest on all of these measures. PVT demonstrated lower CBF reliability, reproducibility and trait specificity than EO and EC. Overall network connectivity reliability was comparable between ASL and BOLD. Our findings confirm ASL CBF as a reliable, stable, and consistent measure of resting-state regional brain function and support the use of EC or EO over FIX and PVT as the resting-state condition.

*Corresponding author. Department of Neurology, University of Pennsylvania, 3W Gates Pavilion, 3400 Spruce Street, Philadelphia, PA, 19104, USA. detre@mail.med.upenn.edu (J.A. Detre).

[1]These authors contributed equally to the work.

Keywords

Arterial spin labeled (ASL) perfusion MRI; Resting state conditions; Reliability; Trait specificity; Network connectivity

Introduction

Resting state fMRI (rs-fMRI) reveals the intrinsic brain activity unrelated to a specific cognitive of sensorimotor task and it is now widely used to characterize the state and trait effects of brain function (Matthews et al., 2006; Sorg et al., 2007; Fox and Raichle, 2007; Raichle, 2015; Bijsterbosch et al., 2017; Detre et al., 2009, 2012). Because **r**esting-state fMRI requires minimal subject engagement, it can easily be acquired in a variety of populations including patients (Power et al., 2014) and, in contrast to task fMRI, can address brain function broadly across multiple domains as subserved by differing brain regions and networks. In general, state effects are studied within subject over time, whereas trait effects are derived from cross-sectional analyses.

Two rs-fMRI techniques, blood oxygen level dependent (BOLD) MRI and arterial spin labeled (ASL) perfusion MRI, have been most commonly used to measure resting brain function. Whereas rs-fMRI based on BOLD contrast detects spatial correlations in spontaneous fluctuations of brain activity as manifested in BOLD signal revealing distributed networks (Fox and Raichle, 2007; Raichle, 2015; Bijsterbosch et al., 2017), it is challenging to interpret the magnitude of resting brain activity since BOLD signal intensity does not provide absolute quantification of cerebral blood flow (CBF) or metabolism. In contrast, ASL MRI can measure resting function directly at the voxel level using magnetically labeled arterial blood water as an endogenous diffusible tracer for quantification of regional CBF (Detre et al., 2009, 2012), which is thought to be coupled to regional neural activity (Raichle, 1998). Static regional CBF (i.e. mean CBF signal averaged across an acquisition) is typically used as a measure of regional brain function (Detre et al., 2009). However, dynamic fluctuations of CBF (e.g. correlations of CBF fluctuations between brain regions) can also be used to assess for spatially correlated changes in brain function in a manner analogous to resting-state BOLD fMRI (Dai et al., 2016).

Resting-state BOLD MRI has been used to identify macroscale brain network organization (Petersen and Sporns, 2015; Power et al., 2014), and functional connectivity metrics have been applied as biomarkers for brain development (Richmond et al., 2016), various disorders (Sheline and Raichle, 2013; Hull et al., 2016; Sheffield and Barch, 2016) and drug effects (Kaczkurkin et al., 2016). Resting-state ASL has also been used to study the neural correlates of state effects such as task (Lim et al., 2010; Poudel et al., 2012) or pharmacological manipulation (Kaczkurkin et al., 2016) as well as trait effects including both genotype (Rao et al., 2007; Franklin et al., 2009) and phenotype (Gianaros et al., 2009).

Although rs-fMRI nominally addresses task-independent brain function, data must be acquired under some task condition, albeit typically low-level, such as eyes closed (EC), eyes open (EO), or visual fixation on a cross-hair (FIX), while the subject lies quietly in the scanner (Power et al., 2014). The specific conditions for rs-fMRI acquisition may influence

regional brain function and its reproducibility. Systematic differences between task conditions have been reported for BOLD rs-fMRI (Marx et al., 2004; Liu et al., 2013; Castellanos et al., 2013). For example, Bianciardi et al. reported substantially higher spontaneous fluctuations of activity in visual areas in EC than FIX (Bianciardi et al., 2009). Dijk et al. compared the EC, EO, FIX and continuous word-classification tasks and reported stronger functional connectivity in default mode and attention networks in EO and FIX than the other tasks (Van Dijk et al., 2010). Patriat et al. compared EC, EO and FIX, and found higher functional connectivity in an auditory network in EC than in the other conditions, greater reliability in FIX than in other conditions of within-network connectivity measurements of default mode, attention and auditory networks, and greater reliability in EO in primary visual network connectivity (Patriat et al., 2013). Tagliazucchi et al. analyzed the functional connectivity of a large publicly available rs-fMRI dataset and reported that EO subjects were less likely to fall asleep during the scan than EC subjects, and FIX subjects had a higher likelihood of staying stably awake (Tagliazucchi and Laufs, 2014). Similarly, using ASL MRI, Hermes et al. reported greater CBF in primary and secondary visual cortex in EO than EC (Hermes et al., 2007). Zou et al. reported higher CBF in primary visual cortex in EO than EC (Zou et al., 2015b), but negligible CBF reliability difference between the two conditions (Zou et al., 2015a). These studies provided valuable insights into the differences between the rs-fMRI conditions, however, systematic comparisons between the commonly used rs-fMRI task conditions are still lacking, especially for ASL MRI.

Understanding how task conditions affect the reliability of rs-fMRI is crucial for developing and optimizing rs-fMRI biomarkers used to elucidate state and trait effects on brain function (Finn et al., 2017). The goal of the present study was to evaluate the effects of specific resting task conditions on ASL MRI, including both mean CBF and the functional correlations in CBF time series, so as to optimize the reliability and sensitivity for detecting state and trait effects on regional brain function. We collected ASL MRI during 4 resting-state task conditions: EC, EO, FIX and PVT (Psychomotor Vigilance Task: a low-level, low-frequency, sustained attention task), at two time points separated by approximately one week in a healthy adult cohort. We used intraclass correlation coefficient (ICC) (Shrout and Fleiss, 1979) and within-subject coefficient of variation (wsCV) to examine the effects of task condition on CBF reliability for detecting state effects, based on the notion that the task condition that would provide the highest sensitivity to state changes across time or trait effects across groups would show the highest ICC and lowest wsCV across repeated measures. In addition, a metric for “trait specificity” (portion of the variance of the observed variable determined by transsituationally consistent and temporally stable trait effects) was derived using latent state-trait (LST) modeling (Steyer et al., 2015), which reflects both the consistency and the stability of the measurements (Hagemann et al., 2002). Previous work using 1.5T ASL data demonstrated high trait specificity of CBF (Hermes et al., 2009). In the present study, we applied the LST model to examine the effects of task condition on trait specificity. For comparison with ASL MRI data, we also acquired resting-state BOLD fMRI under a single resting-state condition (FIX) that was previously suggested to maximize resting-state BOLD retest reliability of default mode, attention and auditory networks (Patriat et al., 2013), and compared the reliability of the network connectivity across the four ASL conditions and BOLD FIX condition.

Methods

Subjects

32 healthy adult subjects (19 female, age = 28.7 ± 4.9 years) with no history of neurologic or psychiatric disorders consented to the study. The study procedures were approved by the University of Pennsylvania Institutional Review Board (IRB). All subjects provided written informed IRB-approved consent prior to participating in the study procedures.

MRI acquisition

The subjects completed two MRI scanning sessions spanning a mean of 7 days. Each session was conducted at the same time of day for each subject, using either a 3T Siemens Trio and 32-channel head array (for N = 14 subjects) or a 3T Siemens Prisma and 64 channel head array (for N = 18 subjects). The same scanner was used for both scans in each subject. The scanning protocol included a 1 mm isotropic T1-MPRAGE structural MRI scan, TOF angiography to guide labeling plane selection, and four 8-min ASL scans obtained with FIX, EO, EC and PVT carried out in pseudorandomized order counterbalanced across subjects and sessions. A single-shot, background-suppressed pseudocontinuous ASL (pCASL) sequence with 90% background suppression, balanced pCASL and an accelerated 3D RARE Stack-Of-Spirals readout was used to collect whole-brain perfusion maps at 3.75 mm isotropic resolution with the following imaging parameters: FOV = 240 × 240 × 128 mm, 34 nominal partitions with 5.9% oversampling, slice PF = 5/8, R = 2 slice acceleration, in-plane matrix = 64 × 64, effective TE = 10.3 ms, TR = 4–4.5s. Each kz partition was divided into two spiral interleaves, with each interleaf acquired sequentially between a separate pair of refocusing RF pulses. The spiral readout trajectories were generated numerically (King et al., 1995), assuming maximum gradient amplitude and slew rate of 36 mT/m and 120 mT/m/ms, respectively, and receiver bandwidth = 400 kHz. A full description can be found in (Vidorreta et al., 2017). 60 control-label pairs of ASL images were collected for each scan (~8 min). A labeling duration and postlabeling delay of 1.8s each were chosen to minimize the sensitivity of CBF quantification to transit time effects in this cohort (Alsop and Detre, 1996; Alsop et al., 2015). An M0 image with no ASL preparation and long TR was also collected for CBF calibration purposes. To better control for possible off-resonance effects that can affect labeling efficiency (Wu et al., 2007), the shimming volume was adjusted to include the chosen labeling location.

An 8-min multiband BOLD-EPI scan was also obtained under FIX condition with the following parameters: TR/TE = 750/30 ms, flip angle 40°, matrix = 76 × 76 on a 192 mm × 192 mm FOV, multiband factor = 6, 66 slices with slice thickness = 2.5 mm, and 641 time points.

The subjects lay supine in the scanner and small cushions were used to secure the subjects' heads to minimize head movements during scanning. The mirror on top of the head coil was adjusted to ensure that the subjects could see the whole screen. The awake status of the subjects was checked by video monitoring and by communications with subjects between scans. Before each resting scan, subjects were instructed through the intercom to either keep their eyes open and fixed on the cross on the screen (FIX), or keep their eyes open without

fixation (EO), or keep their eyes closed (EC), or keep their eyes on the screen and press the response button when a visual stimulus appeared on the screen (PVT).

8 subjects including 1 subject who fell asleep during the scan, and 7 other subjects who showed excessive head motion (mean relative motion >0.3 mm) or low SNR images (global temporal SNR <3.33) were discarded. The images of the remaining 24 subjects (14 female, age = 29.0 ± 5.2 years) were analyzed in the study. Three of the twenty-four subjects did not complete all 4 ASL task conditions, so their data were only used for the within-condition analysis.

ASL data preprocessing

The raw ASL and M0 images were realigned and registered to the anatomical dataset using FSL (Jenkinson et al., 2012) and custom scripts in Matlab. Subtracted [control-label] volume pairs were converted into CBF units following the one-compartment model using assumed values for labeling efficiency and blood T1 relaxation (Alsop et al., 2015). The CBF images were then normalized into MNI space using FSL. For simplicity, we denote the CBF time series as the time series of calculated CBF images of each scan, and denote the CBF maps as the mean CBF image of each scan in the following sections.

Regions of interest (ROI) examined in prior work on ASL retest reliability (Hermes et al., 2009) were defined using published templates (Tzourio-Mazoyer et al., 2002; Tatu et al., 1998). These include whole-brain gray and white matter regions, the four cerebral lobes, the arterial vascular territories, and multiple specific cortical and subcortical GM regions (Table 1). The mean CBF of the selected ROIs as well as the global mean CBF were extracted from the CBF maps.

CBF reproducibility and reliability analysis

The reproducibility and reliability across sessions and across conditions were assessed using the within-subject coefficient of variance (wsCV) and the intraclass correlation coefficient (ICC), respectively, for global mean CBF and the mean CBF of selected ROIs. The differences across sessions and conditions were assessed via permutation tests with a paired sample design.

To assess data quality, the temporal SNR (tSNR) and mean Gray matter-White matter (GM-WM) contrast ratio were computed for each scan and compared across sessions and conditions.

CBF latent state-trait analysis

To test the consistency and stability of CBF measures, we evaluated the trait specificity of CBF for the 4 task conditions using the LST model. Latent state-trait theory has been applied in various domains, especially psychology (Steyer et al., 2015). LST decomposes observable variables into the sum of latent trait variables (personal attributes), state residuals (person-situation interaction), and measurement errors (Steyer et al., 2015). A previous study estimated both the LST model and the latent-trait model (LT model, which decomposes observable variables into the sum of latent trait variables and the measurement

errors, and presumes that there are no occasion-specific effects) on ASL data acquired on a 1.5T MRI scanner, and demonstrated that the mean CBF of most regions of interest accepted the LST model and the mean CBF had high trait specificity, whereas only a few regions of interest accepted the LT model (Hermes et al., 2009). Acceptance of the latent state-trait model means that the model adequately explains the underlying structure of the observed CBF data, as defined by statistical significance (defined below).

In the present study, the LST models were implemented with R toolbox "lsttheory" (Steyer et al., 2015) and "lavaan" (Rosseel, 2012). To fit the data to the LST model, first each 8-min ASL scan was divided into two measurement halves. The mean CBF maps were calculated for each half and shuffled to avoid order effects. Both ROI-based (Table 1) and whole-brain voxel-based LST models (Fig. 1A) were estimated. For LST modeling, we treated the CBF values as the observed variables Y_{ik} (Fig. 1) (Steyer et al., 1999)(Hermes et al., 2009), where indices i and k indicate measurement and session, respectively. The LST model decomposes the observed variable Y_{ik} into the sum of a measurement error variable ε_{ik} and the true score variable τ_{ik}, i.e. the latent state variable, which is further decomposed into the sum of a latent trait component ξ_{ik} and a latent state residual ζ_{ik}, to reflect the situation and/or person-situation interaction effects (Steyer et al., 1999):

$$Y_{ik} = \varepsilon_{ik} + \tau_{ik} = \varepsilon_{ik} + \xi_{ik} + \zeta_{ik}$$

The measurement error, the latent state residual, and the latent trait are un-correlated with each other. The variance of each observed variable can be decomposed into the variances of the measurement error, trait component and latent state residual (Steyer and Schmitt, 1990; Steyer et al., 1999):

$$Var(Y_{ik}) = Var(\varepsilon_{ik}) + Var(\tau_{ik}) = Var(\varepsilon_{ik}) + Var(\xi_{ik}) + Var(\zeta_{ik})$$

Inspired by the work of Hermes et al. (2009), a restrictive LST model equating the measurement error variance, state residual variance, and effects of trait and states in the model was used in the current study.

The structural equation of the LST model was created with "lsttheory" toolbox (Steyer et al., 2015), and the model was then estimated with the confirmatory factor analysis (CFA) using the maximum likelihood algorithm (ML) implemented in the structural equation modeling (SEM) package "lavaan" (Rosseel, 2012) to maximize the likelihood between the estimated variance-covariance matrices of the model ($\widehat{Cov(Y)}$) and the actual variance-covariance matrices of the observed variables ($Cov(Y)$). An LST model was only accepted when the critical ratios ($C.R.$) of the estimated model parameters (variance of trait $Var(\xi_{ik})$, variance of state residual $Var(\zeta_{ik})$ and variance of measurement error $Var(\varepsilon_{ik})$) to their corresponding standard errors ($S.E.$) were statistically significant ($C.R. = Var/S.E.;\ \alpha = 0.05$), and the discrepancy between estimated variance-covariance matrices of the model ($\widehat{Cov(Y)}$) and the variance-covariance matrices of the observed data ($Cov(Y)$) was not significant (assessed by $Chi-square\ \chi^2 test;\ \alpha = 0.05$) (Hermes et al., 2009).

Trait specificity was calculated dividing the estimated variance of the trait component by the variance of the observed variable (Steyer et al., 2015; Hagemann et al., 2002):

$$Trait\ specificity = Var(\xi_{ik})/Var(Y_{ik})$$

The trait specificity ranges from 0 to 1, and it is unitless. It represents the portion of variance of the observed CBF that is determined by temporally stable and transsituationally consistent individual differences, hence is likely to represent phenotype effects. Higher trait specificity denotes higher consistency and stability of the measured trait effects.

A single grouped LST model (Fig. 1B) was additionally used to compare the trait effects between the four conditions, combining the CBF measurements of the four conditions as four groups and more stringently assuming the model to have equal measurement error variance and equal state residual variance across the conditions, so that the trait effects can be compared between the conditions more directly.

Network connectivity analysis

To compare the reliability of network connectivity across the resting ASL conditions and BOLD data, we evaluated the mean within-network connectivity strength and the mean ICC of the within-network connections (Patriat et al., 2013) using the 264-node network atlas provided in the 2011 study by Power et al. (2011).

The resting BOLD data were preprocessed following the functional connectivity analysis pipeline in (Biswal et al., 2010) using FSL (Jenkinson et al., 2012) and AFNI (Cox, 2012). The BOLD data was band-pass filtered (0.009–0.1 Hz). We regressed out the mean white matter (eroded mask), CSF, and global signals, as well as the motion parameters, for both BOLD time series and the CBF time series of each ASL task condition. Because of the controversy regarding the usage of the global signal as regressor in functional connectivity analyses (Murphy et al., 2009), we also conducted a sensitivity analysis that did not include the global signal as a confound (see supplementary material).

Because the cerebellum region and the top of the brain were not covered well for some of subjects during the ASL scans, we created a common brain mask across the subjects by taking the intersection of their skull stripped (Smith, 2002) and normalized brain mask of the mean ASL image. We eliminated the ROIs in the cerebellum region as well as the ROIs outside of our common brain mask in the 264-node network atlas (Power et al., 2011), leaving 215 ROIs of 12 distinctive cerebral rs-fMRI networks for the network connectivity analysis (Supplementary Table S1 and Supplementary Fig. S1). The mean time series of the network ROIs were extracted and Pearson's r correlation coefficient between each pair of ROIs was calculated and transformed to Z scores using Fisher's r-to-z transformation (Fisher, 1921) to form a connectivity matrix for each BOLD and ASL time series. The ties of nearby ROIs (<20 mm) were terminated and an 8% tie density mask was created to retain the strongest correlations for each condition (Power et al., 2011). An intersection mask of the tie masks was generated and the connections in the intersection mask were used in analysis described below.

The mean connectivity strength within each network was calculated for each scan of the 5 conditions (BOLD FIX and the 4 ASL conditions) and a 12 × 5 two-way repeated measures ANOVA (Networks x resting conditions) was used to examine the effects of network and resting condition on the within-network connectivity strength. The mean connectivity strength of all within-network connections, as well as the mean connectivity strength within each network was further compared between each pair of conditions using paired T-tests. To evaluate their reliability, the ICC of each within-network connection was calculated and the ICC values were averaged within each network, as well as across all the within-network connections, for each task condition. Differences in the averaged ICCs were then assessed between the task conditions using a paired Jackknife leave-one-out resampling method (Patriat et al., 2013). Briefly, one subject was left out each time, and the averaged ICC was computed for the within network connections for each condition. The averaged ICCs of all possible leave-one-out samples were collected and compared between the conditions using the paired T test. The paired T test results of mean connectivity strength and averaged ICCs were thresholded at $p < 0.05$, Bonferroni corrected for the number of comparisons (13 'networks and all within network' x 10 combinations of the task conditions).

Results

Reproducibility and reliability of mean CBF

No significant difference was found in global mean CBF across sessions. Excellent within-session agreement was observed for both scan sessions (wsCV <5%, ICC >0.9) (Fig. 2, row 1).

Significant differences in reproducibility and reliability were found across the four task conditions. The global mean CBF of EC was significantly higher than the other task conditions (Fig. 2, D). FIX condition presented significantly higher wsCV than EC, and significantly lower ICC than the other 3 task conditions, suggesting lower reproducibility and reliability compared to the other task conditions (Fig. 2, E and F). Similar reproducibility and reliability patterns were also shown for the mean CBF within selected ROIs, as listed in Tables 2 and 3.

The global tSNR and the GM-WM contrast ratios were similar between the two scan sessions (Fig. 3, A and B). The global tSNR of EC condition was smaller than FIX and PVT; however there was no difference in GM-WM contrast ratio between the four conditions (Fig. 3, C and D).

Latent state-trait model

The restrictive LST model was accepted for most ROIs for each of the conditions (Fig. 4). The derived trait specificities of regional CBF were mostly larger than 0.7 for the four task conditions. EC yielded the highest trait specificity (range 0.77–0.87), while FIX showed the lowest trait specificity (range 0.56–0.81).

Voxel-wise estimation of the LST model demonstrated that most brain voxels accepted the restrictive LST model (Supplementary Fig. S2). FIX showed distinctly lower trait specificity than the other conditions.

The single grouped LST model which nested the 4 task conditions and further assumed equal measurement error variance and equal state residual variance across the conditions was accepted for all ROIs (Supplementary Fig. S3). In the single grouped model, the estimated trait specificity for FIX was again lower than other conditions for most ROIs. Compared to the separated model (Fig. 4), differences between FIX and other conditions were reduced, likely due to assuming equal state residual variance across all conditions in the single grouped model.

Network connectivity strength and reliability

A 12 × 5 two-way repeated measures ANOVA (networks x resting conditions) on the mean within-network connectivity strength examined here found significant effects of network ($p < 0.0001$) and resting condition ($p = 0.026$). Paired T-tests between the conditions showed that the within-network connectivity strength was generally similar across all 4 ASL task conditions, however EO and EC demonstrated stronger connectivity than PVT in the visual network, and EO presented higher mean connectivity strength of all within-network connections than PVT (Fig. 5A). There were no significant differences between the measured network strength of BOLD FIX and that for the 4 ASL task conditions in most networks. BOLD FIX only presented higher connectivity in the sensory/somatomotor mouth network than the 4 ASL conditions, higher connectivity in the default mode network than ASL EO and ASL EC, and lower connectivity in the salience network than ASL EO and ASL EC (Fig. 5A).

The mean ICCs across all within-network connections were not significantly different between the ASL EO, EC and PVT, while ASL FIX demonstrated significantly lower ICC than the other 3 ASL conditions (Fig. 5B, leftmost group of bars). When broken down into different networks, the mean ICC's were significantly different across conditions (Fig. 5B). For example, ASL EO presented the highest reliability in the visual, ventral attention and dorsal attention networks; ASL EC presented the highest reliability in the cingulo-opercular task control, auditory, memory retrieval, and salience networks; ASL PVT presented highest reliability in the sensory/somatomotor hand, default mode, and frontoparietal task control networks; ASL FIX and PVT shared higher reliability in the sensory/somatomotor mouth network; ASL FIX, EO and PVT demonstrated higher reliability than ASL EC in the subcortical network.

The mean ICC across all within-network connections of BOLD FIX was significantly higher than that of ASL FIX but wasn't significantly different than the other 3 ASL conditions, and showed no consistent trend across different networks (Fig. 5B). The relationship between the ICC and connectivity strength is also illustrated in Supplementary Fig. S4 for each network and each connection tie.

Similar within-network connectivity strength and reliability results were obtained when data were preprocessed without global signal regression (Supplementary Fig. S5 and Fig. S6). Without global signal regression, the averaged ICC across all within-network connections slightly and gradually increased from ASL FIX to ASL EO, and to ASL EC, while the averaged ICC of ASL PVT was lower than the other 3 ASL conditions. There was no

significant difference between the averaged ICC across all within-network connections of BOLD FIX and that of ASL FIX (Supplementary Fig. S5B, leftmost group of bars).

Discussion

We investigated the effects of 4 different resting task conditions (FIX, EO, EC and PVT) on the reproducibility and trait specificity of ASL mean CBF, and on the reliability of ASL CBF network connectivity. Retest reproducibility was examined to help guide resting-state ASL task selection for repeated measures designs using CBF as a biomarker of intervention effects, while trait specificity was examined to provide additional guidance on resting-state ASL task selection for cross sectional studies using CBF as a biomarker of genotype and phenotype effects.

In accordance with previous studies (Chen et al., 2011; Jain et al., 2012; Jahng et al., 2005; Hodkinson et al., 2013; Zou et al., 2015a; Almeida et al., 2018), our results demonstrated excellent retest reliability of both mean and regional CBF for all the four resting conditions. Among the 4 resting conditions, FIX presented the lowest retest reliability, while EC yielded higher (but not significantly) reliability and reproducibility than EO and PVT. The lower ICC and higher wsCV of FIX suggests higher within-subject variability of mean CBF in the FIX condition. Accordingly, repeated measures designs using resting-state ASL to detect changes in regional CBF and brain function might be optimized by using a resting-state task other than FIX. A slightly increased mean CBF in EC as compared to other conditions along with increased between-subject variance and reduced within-subject variance (Table 3 and Supplementary Table S2) may explain the increased ICC and reduced wsCV observed for EC versus the other conditions. However, a limitation of EC is the challenge in distinguishing EC awake from EC asleep.

The lower global tSNR of EC (Fig. 3) was driven by the higher global fluctuation in EC than other conditions (Supplementary Fig. S7). This was in agreement with earlier literature reporting higher spontaneous fluctuations of brain activity in EC than EO using BOLD fMRI (Bianciardi et al., 2009), and the decrease in BOLD rs-fMRI global signal amplitude from EC state to EO state was correlated with the increase of EEG vigilance (Wong et al., 2016). The higher amplitude of fluctuation in EC versus EO may be attributed to the different levels of BOLD and CBF in deactivated states of these two conditions, as has been reported previously (Uludag et al., 2004).

Consistent with prior work (Hermes et al., 2009), most of the brain regions examined also accepted the latent state-trait model, suggesting that the LST model could adequately explain the underlying structure of CBF data and confirming that resting CBF can be effectively decomposed into trait-like factors, measurement errors and situational effects. The latter include both physiological effects (such as hormonal status) and psychological effects (such as anxiety) which may influence the mean CBF in each scan session (Hermes et al., 2009). Four regions in EC or PVT conditions failed to accept the LST model (white grids of Fig. 4), suggesting that the estimated model didn't fit the measured data well. This might be a result of the maximally restricted model criteria: equal effects of traits, equal effects of states, equal measurement error variance and equal state residual variance.

Relaxation of these restrictions would provide a better model fit to the data (Schmitt and Steyer, 1993; Hagemann et al., 2002). The trait specificity reflects both consistency and stability (Hagemann et al., 2002). We found that trait specificity of the selected ROIs was mostly >0.7 for the 4 resting conditions, suggesting >70% of the observed mean CBF variance were determined by trans-situationally consistent and temporally stable individual differences. Among the 4 resting conditions, EC yielded the highest trait specificity (77%–87%), EO (69%–85%) was slightly lower than EC, and FIX was the lowest (56%–81%). These results suggest that ASL CBF measured during EC and EO provides a more stable and consistent proxy for trait effects of CBF, and that FIX is more vulnerable to situational effects than the other three conditions.

As has previously been shown for BOLD data (Patriat et al., 2013), there were no significant differences in mean within-network connectivity strength between the 4 ASL conditions for most of the networks studied, except in the visual network, where EO and EC showed higher connectivity than PVT. The mean reliability of within-network connections wasn't significantly different between ASL EO, EC and PVT, while ASL FIX demonstrated lower reliability than the other 3 conditions. However at the individual network level, some differences in reliability were observed across resting-state conditions. Our findings for resting-state ASL data are contrary to previous BOLD findings (Patriat et al., 2013), which suggested greater reliability in FIX than EO and EC in default mode, attention and auditory networks, and greater reliability in EO in primary visual network connectivity. Potential factors contributing to this difference include imaging modality, acquisition parameters, image processing procedures, effects of the pairwise subtraction in ASL, and ROI selection (215 ROIs vs 18 ROIs). Unfortunately, we were not able to repeat all of the resting-state conditions with BOLD acquisitions for comparison with ASL data, so we are unable to determine which resting-state condition optimized resting-state BOLD reproducibility in our cohort. However, without including the global signal as nuisance variable in the nuisance regression of preprocessing to match the previous study (Patriat et al., 2013), our data showed that FIX yielded highest reliability of default mode network together with EC, while EO remained more reliable in the visual network (Supplementary Fig. S5).

The mean connectivity strength of all within-network connections for BOLD resting data acquired during FIX was similar with that of ASL data. There was no significant difference between BOLD FIX and ASL EO, EC and PVT in the average reliability of all within-network connections when global signal regression was included in preprocessing (Fig. 5B), or between BOLD FIX and ASL FIX when global signal regression was not performed (Supplementary Fig. S5B), suggesting that the overall network reliability was comparable between these two modalities. While ASL provides a direct measure of CBF, BOLD contrast indirectly reflects a complex interaction between changes in CBF, cerebral blood volume, cerebral metabolic rate of oxygen (Detre and Wang, 2002; Buxton et al., 2004). As previously mentioned, acquisition parameters such as the voxel size and time resolution were also different between the two imaging modalities; and the processing steps such as the pairwise subtraction in ASL could also contribute to differences in network connectivity between ASL and BOLD.

Resting-state functional connectivity relies on low frequency correlations in spontaneous fluctuations of brain activity (Cordes et al., 2001), and can be can be reliably detected with ASL (Chuang et al., 2008; Viviani et al., 2011; Zhu et al., 2013; Dai et al., 2016; Zou et al., 2015a). Although the effective TR = 8s of the ASL CBF time series in the present study is much longer than the BOLD TR, it corresponds to a frequency band between 0 and 0.06 Hz, which is very similar to the commonly used frequency band of ~0.01–0.1 Hz used to filter resting-state BOLD fMRI data for connectivity analysis. The pair-wise subtraction in ASL CBF quantification also reduces low-frequency noise inherent in BOLD fMRI data, making ASL a particularly useful tool for investigation of slow brain activity fluctuations (Aguirre et al., 2002; Wang et al., 2008). Prior work has demonstrated that ASL MRI can detect resting-state correlations at very low frequencies (Niazy et al., 2011).

A limitation of this study is that 60 sampled CBF time points may be suboptimal for connectivity analyses, though prior work has successfully identified resting-state networks with even smaller times series (Zhu et al., 2013; Dai et al., 2016). The temporal resolution of current ASL approaches is fundamentally limited by the time required for labeling and post-labeling delays, and by the need for two images (control and label) to generate the perfusion contrast. However, ASL temporal resolution can be doubled with careful attention to background and artifact suppression resulting in a single image in which the contrast is almost purely CBF (Zhao et al., 2017). Factors such as morning-evening variation (Shannon et al., 2013) and scan order (Yan et al., 2009) may also influence CBF and network connectivity, but in the present study, images were collected at the same time of day for the two visits and the four ASL conditions were scanned in a pseudorandomized order counterbalanced across the subjects and visits.

Global signal regression is a controversial preprocessing step in connectivity analysis, and our recent findings suggest that a global network represents a sizeable portion of brain connectivity measured by ASL MRI (Zhao et al., 2017). Accordingly, we examined connectivity both with and without global signal regression (Murphy and Fox, 2017). Lastly, given the immense sleep pressure in resting studies (Tagliazucchi and Laufs, 2014), subjects may fall asleep during scanning. We verified awake status by video monitoring and by communications with subjects between scans, but it is conceivable that some subjects still fell asleep during the EC scans.

In the present study, EC presented the highest CBF reliability, reproducibility, trait specificity, and network connectivity reliability for resting-state ASL data, followed by EO, whilst FIX showed the lowest on these measures. The poorer reliability of FIX might be attributable to variations in strategic behavior of subjects during the FIX scan to fight sleep and boredom and to adhere to fixating on the target (Tagliazucchi and Laufs, 2014). PVT demonstrated lower CBF reliability, reproducibility and trait specificity than EO and EC, and similar network connectivity reliability with EC and EO (and lower network connectivity reliability than EC, EO and FIX when global signal regression was not performed). These differences might be attributed to practice effects (Jolles et al., 2010). Given the higher reliability in CBF and network connections, and better proxy to the CBF trait, our results support the use of EC or EO over FIX and PVT for resting-state ASL.

Because of the challenges in verifying awake status during EC, EO may be preferable as awake status can be easily verified using video monitoring.

Conclusion

This study confirmed ASL CBF as a reliable, stable, and consistent measure of regional CBF and physiological trait effects in brain function, and provided a reference for choosing optimal conditions for future studies. Our findings suggest that EC and EO are more reliable conditions for both repeated measures of ASL CBF and for detecting trait-like effects in regional brain function.

Supplementary Material

Refer to Web version on PubMed Central for supplementary material.

Acknowledgments

This work was supported by NIH grants MH080729 and EB015893. DCA is an inventor of pseudocontinuous ASL and receives a share of postmarket royalties from his institution's licenses to GE Healthcare, Philips Healthcare, Siemens Healthineers, Hitachi Medical, and Animage LLC.

References

Aguirre G, Detre J, Zarahn E, Alsop D. Experimental design and the relative sensitivity of BOLD and perfusion fMRI. Neuroimage. 2002; 15:488–500. [PubMed: 11848692]

Almeida JRC, Greenberg T, Lu H, Chase HW, Fournier J, Cooper CM, Deckersbach T, Adams P, Carmody T, Fava M, Kurian B, McGrath PJ, McInnis M, Oquendo MA, Parsey R, Weissman M, Trivedi M, Phillips ML. Test-retest reliability of cerebral blood flow in healthy individuals using arterial spin labeling: findings from the EMBARC study. Magn Reson Imaging. 2018; 45:26–33. [PubMed: 28888770]

Alsop DC, Detre JA. Reduced transit-time sensitivity in noninvasive magnetic resonance imaging of human cerebral blood flow. J Cerebr Blood Flow Metabol : Offic J Int Soc Cerebr Blood Flow Metabol. 1996; 16:1236–1249.

Alsop DC, Detre JA, Golay X, Gunther M, Hendrikse J, Hernandez-Garcia L, Lu H, MacIntosh BJ, Parkes LM, Smits M, van Osch MJ, Wang DJ, Wong EC, Zaharchuk G. Recommended implementation of arterial spin-labeled perfusion MRI for clinical applications: a consensus of the ISMRM perfusion study group and the European consortium for ASL in dementia. Magn Reson Med. 2015; 73:102–116. [PubMed: 24715426]

Bianciardi M, Fukunaga M, van Gelderen P, Horovitz SG, de Zwart JA, Duyn JH. Modulation of spontaneous fMRI activity in human visual cortex by behavioral state. Neuroimage. 2009; 45:160–168. [PubMed: 19028588]

Bijsterbosch, J., Smith, SM., Beckmann, CF. An Introduction to Resting State FMRI Functional Connectivity. Oxford University Press; 2017.

Biswal BB, Mennes M, Zuo XN, Gohel S, Kelly C, Smith SM, Beckmann CF, Adelstein JS, Buckner RL, Colcombe S, Dogonowski AM, Ernst M, Fair D, Hampson M, Hoptman MJ, Hyde JS, Kiviniemi VJ, Kotter R, Li SJ, Lin CP, Lowe MJ, Mackay C, Madden DJ, Madsen KH, Margulies DS, Mayberg HS, McMahon K, Monk CS, Mostofsky SH, Nagel BJ, Pekar JJ, Peltier SJ, Petersen SE, Riedl V, Rombouts SA, Rypma B, Schlaggar BL, Schmidt S, Seidler RD, Siegle GJ, Sorg C, Teng GJ, Veijola J, Villringer A, Walter M, Wang L, Weng XC, Whitfield-Gabrieli S, Williamson P, Windischberger C, Zang YF, Zhang HY, Castellanos FX, Milham MP. Toward discovery science of human brain function. Proc Natl Acad Sci USA. 2010; 107:4734–4739. [PubMed: 20176931]

Buxton RB, Uludag K, Dubowitz DJ, Liu TT. Modeling the hemodynamic response to brain activation. Neuroimage. 2004; 23(Suppl 1):S220–S233. [PubMed: 15501093]

Castellanos FX, Di Martino A, Craddock RC, Mehta AD, Milham MP. Clinical applications of the functional connectome. Neuroimage. 2013; 80:527–540. [PubMed: 23631991]

Chen Y, Wang DJ, Detre JA. Test-retest reliability of arterial spin labeling with common labeling strategies. J Magn Reson Imag : JMRI. 2011; 33:940–949.

Chuang KH, van Gelderen P, Merkle H, Bodurka J, Ikonomidou VN, Koretsky AP, Duyn JH, Talagala SL. Mapping resting-state functional connectivity using perfusion MRI. Neuroimage. 2008; 40:1595–1605. [PubMed: 18314354]

Cordes D, Haughton VM, Arfanakis K, Carew JD, Turski PA, Moritz CH, Quigley MA, Meyerand ME. Frequencies contributing to functional connectivity in the cerebral cortex in "resting-state" data. AJNR Am J Neuroradiol. 2001; 22:1326–1333. [PubMed: 11498421]

Cox RW. AFNI: what a long strange trip it's been. Neuroimage. 2012; 62:743–747. [PubMed: 21889996]

Dai W, Varma G, Scheidegger R, Alsop DC. Quantifying fluctuations of resting state networks using arterial spin labeling perfusion MRI. J Cerebr Blood Flow Metabol : Offic J Int Soc Cerebr Blood Flow Metabol. 2016; 36:463–473.

Detre JA, Rao H, Wang DJ, Chen YF, Wang Z. Applications of arterial spin labeled MRI in the brain. J Magn Reson Imag : JMRI. 2012; 35:1026–1037.

Detre JA, Wang J. Technical aspects and utility of fMRI using BOLD and ASL. Clin Neurophysiol : Offic J Int Fed Clin Neurophysiol. 2002; 113:621–634.

Detre JA, Wang J, Wang Z, Rao H. Arterial spin-labeled perfusion MRI in basic and clinical neuroscience. Curr Opin Neurol. 2009; 22:348–355. [PubMed: 19491678]

Finn ES, Scheinost D, Finn DM, Shen X, Papademetris X, Constable RT. Can brain state be manipulated to emphasize individual differences in functional connectivity? Neuroimage. 2017

Fisher RA. On the probable error of a coefficient of correlation deduced from a small sample. Metron. 1921; 1:3–32.

Fox MD, Raichle ME. Spontaneous fluctuations in brain activity observed with functional magnetic resonance imaging. Nature reviews Neuroscience. 2007; 8:700–711. [PubMed: 17704812]

Franklin TR, Lohoff FW, Wang Z, Sciortino N, Harper D, Li Y, Jens W, Cruz J, Kampman K, Ehrman R, Berrettini W, Detre JA, O'Brien CP, Childress AR. DAT genotype modulates brain and behavioral responses elicited by cigarette cues. Neuropsychopharmacol : Offic Publ Am Coll Neuropsychopharmacol. 2009; 34:717–728.

Gianaros PJ, Sheu LK, Remo AM, Christie IC, Crtichley HD, Wang J. Heightened resting neural activity predicts exaggerated stressor-evoked blood pressure reactivity. Hypertension. 2009; 53:819–825. [PubMed: 19273741]

Hagemann D, Naumann E, Thayer JF, Bartussek D. Does resting electroencephalograph asymmetry reflect a trait? an application of latent state-trait theory. J Pers Soc Psychol. 2002; 82:619–641. [PubMed: 11999928]

Hermes M, Hagemann D, Britz P, Lieser S, Bertsch K, Naumann E, Walter C. Latent state-trait structure of cerebral blood flow in a resting state. Biol Psychol. 2009; 80:196–202. [PubMed: 18838099]

Hermes M, Hagemann D, Britz P, Lieser S, Rock J, Naumann E, Walter C. Reproducibility of continuous arterial spin labeling perfusion MRI after 7 weeks. Magn Reson Mater Phys Biol Med. 2007; 20:103–115.

Hodkinson DJ, Krause K, Khawaja N, Renton TF, Huggins JP, Vennart W, Thacker MA, Mehta MA, Zelaya FO, Williams SC, Howard MA. Quantifying the test-retest reliability of cerebral blood flow measurements in a clinical model of on-going post-surgical pain: a study using pseudo-continuous arterial spin labelling. NeuroImage Clin. 2013; 3:301–310. [PubMed: 24143296]

Hull JV, Jacokes ZJ, Torgerson CM, Irimia A, Van Horn JD. Resting-state functional connectivity in autism spectrum disorders: a review. Front Psychiatr. 2016; 7:205.

Jahng GH, Song E, Zhu XP, Matson GB, Weiner MW, Schuff N. Human brain: reliability and reproducibility of pulsed arterial spin-labeling perfusion MR imaging. Radiology. 2005; 234:909–916. [PubMed: 15734942]

Jain V, Duda J, Avants B, Giannetta M, Xie SX, Roberts T, Detre JA, Hurt H, Wehrli FW, Wang DJ. Longitudinal reproducibility and accuracy of pseudo-continuous arterial spin-labeled perfusion

MR imaging in typically developing children. Radiology. 2012; 263:527–536. [PubMed: 22517961]

Jenkinson M, Beckmann CF, Behrens TE, Woolrich MW, Smith SM. FSL. Neuroimage. 2012; 62:782–790. [PubMed: 21979382]

Jolles DD, Grol MJ, Van Buchem MA, Rombouts SA, Crone EA. Practice effects in the brain: changes in cerebral activation after working memory practice depend on task demands. Neuroimage. 2010; 52:658–668. [PubMed: 20399274]

Kaczkurkin AN, Moore TM, Ruparel K, Ciric R, Calkins ME, Shinohara RT, Elliott MA, Hopson R, Roalf DR, Vandekar SN. Elevated amygdala perfusion mediates developmental sex differences in trait anxiety. Biol Psychiatr. 2016; 80:775–785.

King KF, Foo TK, Crawford CR. Optimized gradient waveforms for spiral scanning. Magn Reson Med. 1995; 34:156–160. [PubMed: 7476073]

Lim J, Wu WC, Wang J, Detre JA, Dinges DF, Rao H. Imaging brain fatigue from sustained mental workload: an ASL perfusion study of the time-on-task effect. Neuroimage. 2010; 49:3426–3435. [PubMed: 19925871]

Liu D, Dong Z, Zuo X, Wang J, Zang Y. Eyes-open/eyes-closed dataset sharing for reproducibility evaluation of resting state fMRI data analysis methods. Neuroinformatics. 2013; 11:469–476. [PubMed: 23836389]

Marx E, Deutschlander A, Stephan T, Dieterich M, Wiesmann M, Brandt T. Eyes open and eyes closed as rest conditions: impact on brain activation patterns. Neuroimage. 2004; 21:1818–1824. [PubMed: 15050602]

Matthews PM, Honey GD, Bullmore ET. Applications of fMRI in translational medicine and clinical practice. Nature reviews Neuroscience. 2006; 7:732–744. [PubMed: 16924262]

Murphy K, Birn RM, Handwerker DA, Jones TB, Bandettini PA. The impact of global signal regression on resting state correlations: are anti-correlated networks introduced? Neuroimage. 2009; 44:893–905. [PubMed: 18976716]

Murphy K, Fox MD. Towards a consensus regarding global signal regression for resting state functional connectivity MRI. Neuroimage. 2017; 154:169–173. [PubMed: 27888059]

Niazy RK, Xie J, Miller K, Beckmann CF, Smith SM. Spectral characteristics of resting state networks. Prog Brain Res. 2011; 193:259–276. [PubMed: 21854968]

Patriat R, Molloy EK, Meier TB, Kirk GR, Nair VA, Meyerand ME, Prabhakaran V, Birn RM. The effect of resting condition on resting-state fMRI reliability and consistency: a comparison between resting with eyes open, closed, and fixated. Neuroimage. 2013; 78:463–473. [PubMed: 23597935]

Petersen SE, Sporns O. Brain networks and cognitive architectures. Neuron. 2015; 88:207–219. [PubMed: 26447582]

Poudel GR, Innes CR, Jones RD. Cerebral perfusion differences between drowsy and nondrowsy individuals after acute sleep restriction. Sleep. 2012; 35:1085–1096. [PubMed: 22851804]

Power JD, Cohen AL, Nelson SM, Wig GS, Barnes KA, Church JA, Vogel AC, Laumann TO, Miezin FM, Schlaggar BL, Petersen SE. Functional network organization of the human brain. Neuron. 2011; 72:665–678. [PubMed: 22099467]

Power JD, Schlaggar BL, Petersen SE. Studying brain organization via spontaneous fMRI signal. Neuron. 2014; 84:681–696. [PubMed: 25459408]

Raichle ME. Behind the scenes of functional brain imaging: a historical and physiological perspective. Proc Natl Acad Sci USA. 1998; 95:765–772. [PubMed: 9448239]

Raichle ME. The brain's default mode network. Annu Rev Neurosci. 2015; 38:433–447. [PubMed: 25938726]

Rao H, Gillihan SJ, Wang J, Korczykowski M, Sankoorikal GM, Kaercher KA, Brodkin ES, Detre JA, Farah MJ. Genetic variation in serotonin transporter alters resting brain function in healthy individuals. Biol Psychiatr. 2007; 62:600–606.

Richmond S, Johnson KA, Seal ML, Allen NB, Whittle S. Development of brain networks and relevance of environmental and genetic factors: a systematic review. Neurosci Biobehav Rev. 2016; 71:215–239. [PubMed: 27590832]

Rosseel Y. lavaan: an R package for structural equation modeling. J Stat Software. 2012; 48:1–36.

Schmitt MJ, Steyer R. A latent state-trait model (not only) for social desirability. Pers Indiv Differ. 1993; 14:519–529.

Shannon BJ, Dosenbach RA, Su Y, Vlassenko AG, Larson-Prior LJ, Nolan TS, Snyder AZ, Raichle ME. Morning-evening variation in human brain metabolism and memory circuits. J Neurophysiol (Bethesda). 2013; 109:1444–1456.

Sheffield JM, Barch DM. Cognition and resting-state functional connectivity in schizophrenia. Neurosci Biobehav Rev. 2016; 61:108–120. [PubMed: 26698018]

Sheline YI, Raichle ME. Resting state functional connectivity in preclinical Alzheimer's disease. Biol Psychiatr. 2013; 74:340–347.

Shrout PE, Fleiss JL. Intraclass correlations: uses in assessing rater reliability. Psychol Bull. 1979; 86:420–428. [PubMed: 18839484]

Smith SM. Fast robust automated brain extraction. Hum Brain Mapp. 2002; 17:143–155. [PubMed: 12391568]

Sorg C, Riedl V, Muhlau M, Calhoun VD, Eichele T, Laer L, Drzezga A, Forstl H, Kurz A, Zimmer C, Wohlschlager AM. Selective changes of resting-state networks in individuals at risk for Alzheimer's disease. Proc Natl Acad Sci USA. 2007; 104:18760–18765. [PubMed: 18003904]

Steyer R, Mayer A, Geiser C, Cole DA. A theory of states and traits–revised. Annu Rev Clin Psychol. 2015; 11:71–98. [PubMed: 25062476]

Steyer R, Schmitt M. The effects of aggregation across and within occasions on consistency, specificity and reliability. Methodika. 1990; 4:58–94.

Steyer R, Schmitt M, Eid M. Latent state–trait theory and research in personality and individual differences. Eur J Pers. 1999; 13:389–408.

Tagliazucchi E, Laufs H. Decoding wakefulness levels from typical fMRI resting-state data reveals reliable drifts between wakefulness and sleep. Neuron. 2014; 82:695–708. [PubMed: 24811386]

Tatu L, Moulin T, Bogousslavsky J, Duvernoy H. Arterial territories of the human brain: cerebral hemispheres. Neurology. 1998; 50:1699–1708. [PubMed: 9633714]

Tzourio-Mazoyer N, Landeau B, Papathanassiou D, Crivello F, Etard O, Delcroix N, Mazoyer B, Joliot M. Automated anatomical labeling of activations in SPM using a macroscopic anatomical parcellation of the MNI MRI single-subject brain. Neuroimage. 2002; 15:273–289. [PubMed: 11771995]

Uludag K, Dubowitz DJ, Yoder EJ, Restom K, Liu TT, Buxton RB. Coupling of cerebral blood flow and oxygen consumption during physiological activation and deactivation measured with fMRI. Neuroimage. 2004; 23:148–155. [PubMed: 15325361]

Van Dijk KR, Hedden T, Venkataraman A, Evans KC, Lazar SW, Buckner RL. Intrinsic functional connectivity as a tool for human connectomics: theory, properties, and optimization. J Neurophysiol (Bethesda). 2010; 103:297–321.

Vidorreta M, Wang Z, Chang YV, Wolk DA, Fernandez-Seara MA, Detre JA. Whole-brain background-suppressed pCASL MRI with 1D-accelerated 3D RARE Stack-Of-Spirals readout. PLoS One. 2017; 12:e0183762. [PubMed: 28837640]

Viviani R, Messina I, Walter M. Resting state functional connectivity in perfusion imaging: correlation maps with BOLD connectivity and resting state perfusion. PLoS One. 2011; 6:e27050. [PubMed: 22073252]

Wang Z, Aguirre GK, Rao H, Wang J, Fernandez-Seara MA, Childress AR, Detre JA. Empirical optimization of ASL data analysis using an ASL data processing toolbox: ASLtbx. Magn Reson Imaging. 2008; 26:261–269. [PubMed: 17826940]

Wong CW, DeYoung PN, Liu TT. Differences in the resting-state fMRI global signal amplitude between the eyes open and eyes closed states are related to changes in EEG vigilance. Neuroimage. 2016; 124:24–31. [PubMed: 26327245]

Wu WC, Fernandez-Seara M, Detre JA, Wehrli FW, Wang J. A theoretical and experimental investigation of the tagging efficiency of pseudocontinuous arterial spin labeling. Magn Reson Med. 2007; 58:1020–1027. [PubMed: 17969096]

Yan C, Liu D, He Y, Zou Q, Zhu C, Zuo X, Long X, Zang Y. Spontaneous brain activity in the default mode network is sensitive to different resting-state conditions with limited cognitive load. PLoS One. 2009; 4:e5743. [PubMed: 19492040]

Zhao L, Alsop DC, Detre JA, Dai W. Global fluctuations of cerebral blood flow indicate a global brain network independent of systemic factors. J Cerebr Blood Flow Metabol : Offic J Int Soc Cerebr Blood Flow Metabol. 2017 271678X17726625.

Zhu S, Fang Z, Hu S, Wang Z, Rao H. Resting state brain function analysis using concurrent BOLD in ASL perfusion fMRI. PLoS One. 2013; 8:e65884. [PubMed: 23750275]

Zou Q, Miao X, Liu D, Wang DJ, Zhuo Y, Gao JH. Reliability comparison of spontaneous brain activities between BOLD and CBF contrasts in eyes-open and eyes-closed resting states. Neuroimage. 2015a; 121:91–105. [PubMed: 26226087]

Zou Q, Yuan BK, Gu H, Liu D, Wang DJ, Gao JH, Yang Y, Zang YF. Detecting static and dynamic differences between eyes-closed and eyes-open resting states using ASL and BOLD fMRI. PLoS One. 2015b; 10:e0121757. [PubMed: 25816237]

Appendix A. Supplementary data

Supplementary data related to this article can be found at https://doi.org/10.1016/j.neuroimage.2018.02.028.

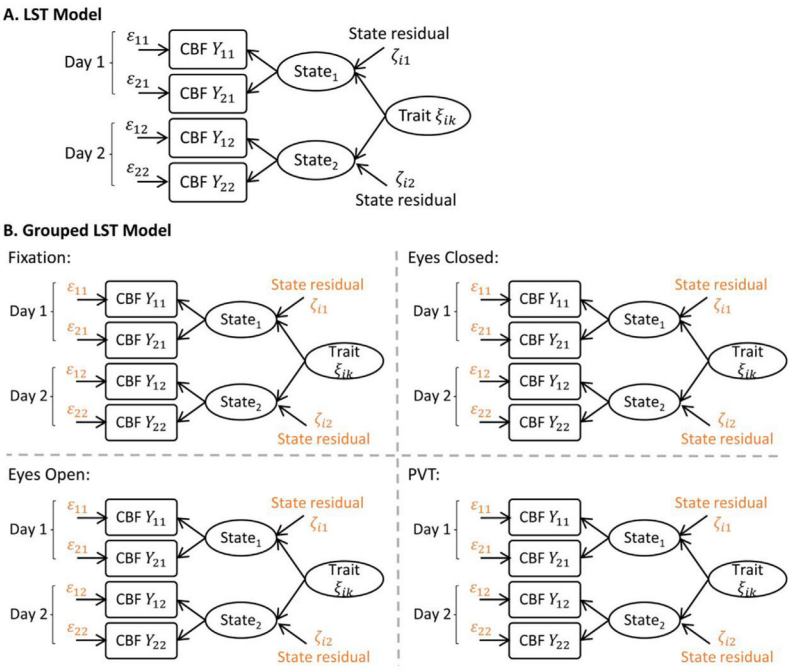

Fig. 1.

Latent State-trait model. (A). The Latent State-trait model (LST) (Steyer et al., 2015) decomposes measured CBF Y_{ik} (ith measure at occasion k) into measurements errors (ε_{ik}) and latent $State_k$. It then further decomposes the latent $State_k$ into state residual (ζ_{ik}) and trait components (ξ_{ik}). The measurement error, the state residual, and the trait are uncorrelated with each other. A restrictive LST model used in this study further assumes equal measurement error variance and equal state residual variance. (B). The grouped LST model nests four models for the four conditions and assumes equal measurement error variance and equal state residual variance across the conditions.

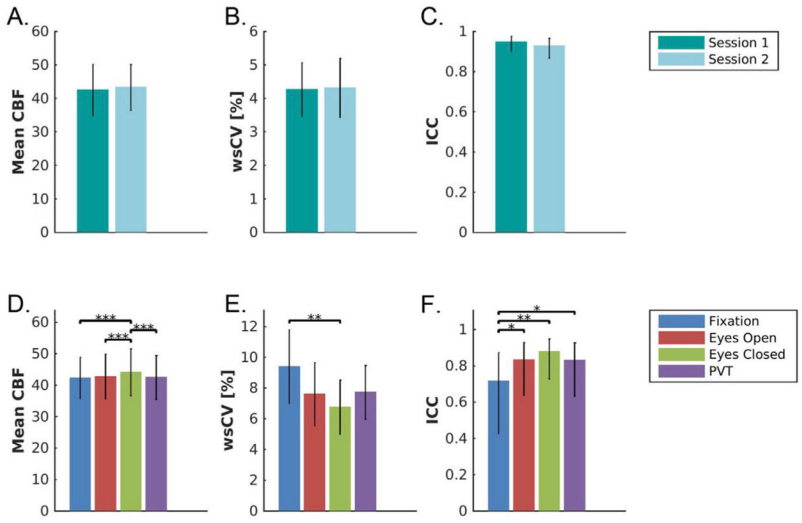

Fig. 2.

Evaluation of global CBF (mean, wsCV and ICC) across scan sessions (Top row) and across task conditions (Bottom row). The global mean CBF was computed for each subject, session and condition, and the within-subject coefficient of variance (wsCV) and the intraclass correlation coefficient (ICC) were then calculated for each session and condition. Fig. 2A and 2D show the global mean CBF and standard deviation across each session and condition, respectively. Fig. 2B and 2E show the wsCV computed across each session and condition, respectively, along with their 95% confidence intervals. Similarly, Fig 2C and 2E how the ICC and theirs 95% confidence interval. Significant differences between each session/condition pairs assessed with permutation tests with a paired sample design are marked with *: $p < 0.05$; **:$p < 0.01$; ***: $p < 0.001$.

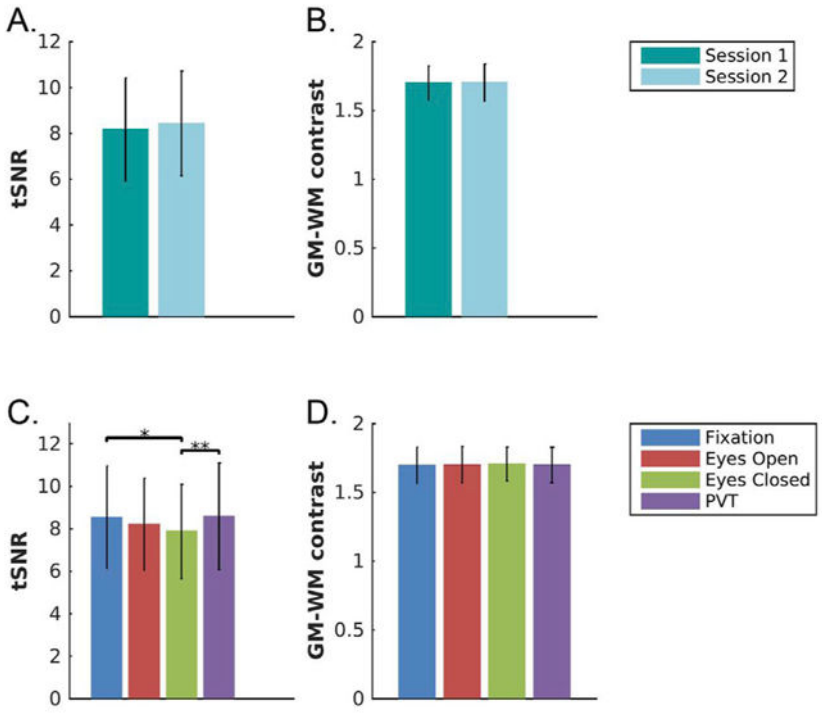

Fig. 3.

tSNR of global CBF and the GM-WM ratio for the scan sessions and conditions. Temporal signal-to-noise-ratio (tSNR) of global mean CBF and the gray matter-white matter (GM-WM) contrast ratio across the two scan sessions (Top Row A and B) and across the four task conditions (Bottom Row C and D). The error bars show the standard deviations for each session/condition. Significant differences between each session/condition pairs assessed with permutation tests with a paired sample design are marked with *: $p < 0.05$; **: $p < 0.01$.

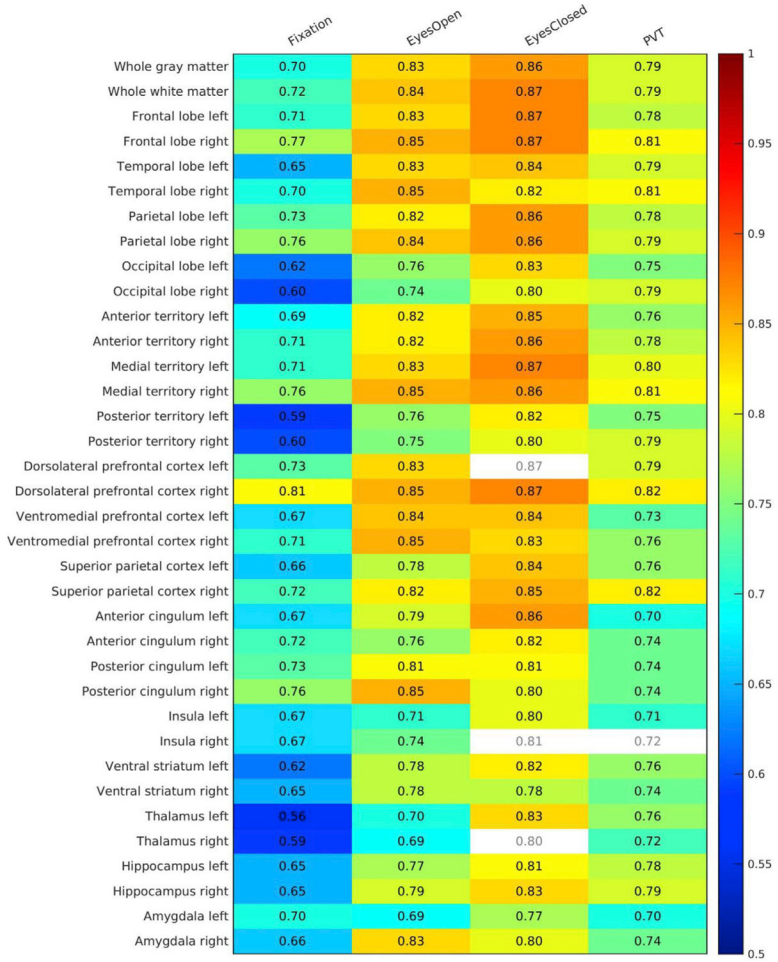

Fig. 4.

Trait specificity of four task conditions: region of interest results. Mean CBF measurements were analyzed separately using the Latent state-trait (LST) model for each of the resting conditions (each column) and each region of interest (ROI, each row). The colored cells are the regions that accepted the restrictive LST model (assuming equal measurement error variance for the measurements and equal state residual variance across the occasions). The labeled values and color scale show the trait specificity of mean CBF estimated by the LST model for each corresponding condition and ROI. Trait specificity ranges from 0 to 1, and is unitless.

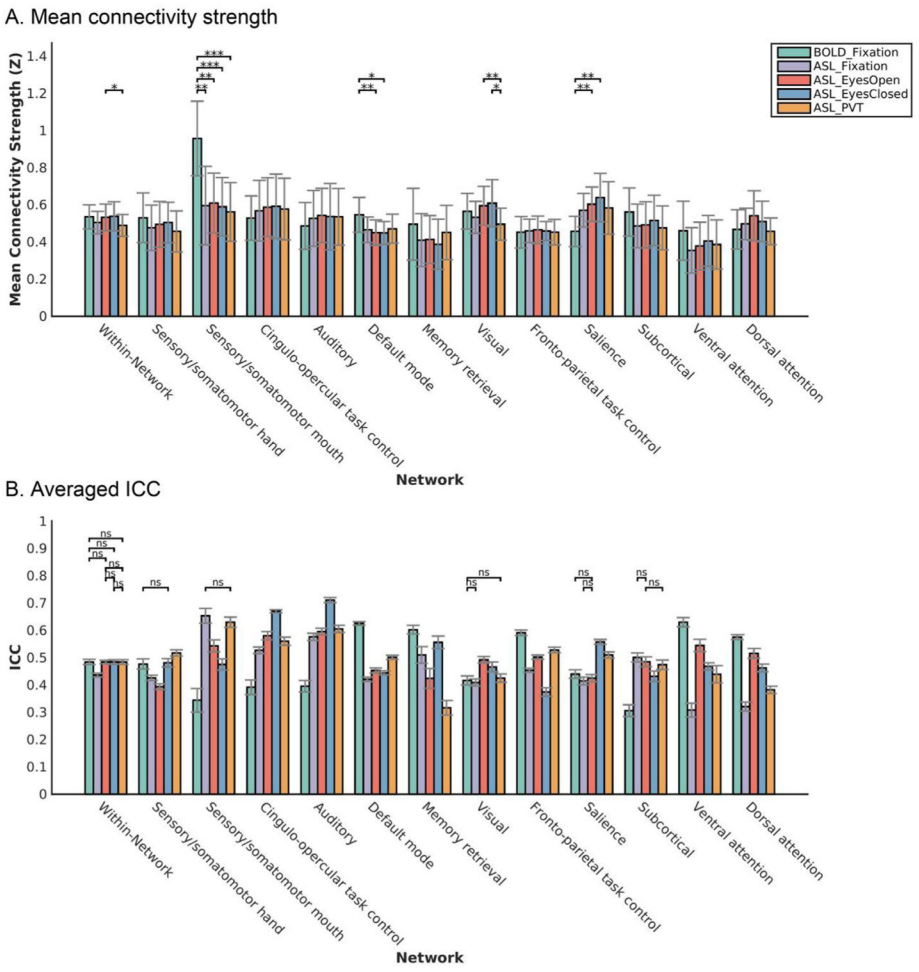

Fig. 5.

Comparison of network connectivity between ASL and BOLD task conditions. (A): the mean connectivity strength of within-network connections. Results are presented across all within-network connections, as well as broken down by networks. The bars and error bars represent the across subject mean and standard deviation of the mean connectivity strength of all within-network connections of the two scan sessions. Significant differences between the conditions were assessed using the paired T test and the Bonferroni corrected p values are marked with *: $p < 0.05$; **: $p < 0.01$; ***: $p < 0.001$. (B): the averaged ICC of within-network connectivity. Results are presented across all within-network connections, as well as broken down by networks. The bars and error-bars show the mean and standard deviation of the averaged ICC of all within-network connections for each task condition using Jackknife leave-one-out resampling method. Significant differences between the conditions were assessed using the paired Jackknife resampling method. Most pairs showed significant differences after Bonferroni correction. For clarity, pairs showing Bonferroni corrected $p > 0.05$ are instead marked as ‘ns’, i.e., non-significant.

Table 1

List of regions of interest (ROIs).

Region of interest	size (cm3)
Whole-brain gray matter	718.32
Whole-brain white matter	741.21
Cerebral Lobes	
Frontal lobe	222.66
Temporal lobe	116.63
Parietal lobe	132.72
Occipital lobe	94.46
Arterial territories	
Anterior cerebral artery (ACA)	135.93
Middle cerebral artery (MCA)	321.9
Posterior cerebral artery (PCA)	100.39
Dorsolateral prefrontal cortex	51.13
Ventromedial prefrontal cortex	25.25
Superior parietal cortex	16.52
Anterior cingulum	8.59
Posterior cingulum	3.14
Insula	14.86
Ventral striatum	1.43
Thalamus	8.72
Hippocampus	7.46
Amygdala	1.76

Table 2

Evaluation of CBF (mean, wsCV and ICC) across scan sessions in the regions of interest (ROI).

Region of interest	Mean CBF(SD)		wsCV [%]		ICC	
	Ses 1	Ses 2	Ses 1	Ses 2	Ses 1	Ses 2
Gray matter	46.83 (8.34)	47.67 (7.39)	4.20	4.34	0.95	0.92
White matter	29.66 (5.58)	30.20 (5.17)	4.23	4.32	0.95	0.94
Frontal lobe	50.70 (8.91)	51.58 (7.91)	3.45	3.99	0.96	0.93
Temporal lobe	45.12 (8.23)	45.68 (7.08)	4.67	5.33	0.93	0.89
Parietal lobe	51.18 (9.26)	52.17 (7.96)	3.97	4.09	0.96	0.93
Occipital lobe	48.48 (9.66)	49.38 (8.48)	7.12	6.68	0.89	0.87
ACA territory	48.07 (8.59)	49.16 (7.71)	3.91	3.96	0.95	0.94
MCA territory	49.95 (8.93)	50.60 (7.62)	3.94	4.51	0.95	0.91
PCA territory	44.86 (8.80)	45.72 (7.89)	6.84	6.37	0.89	0.88
Dorsolateral prefrontal cortex	53.04 (9.51)	53.89 (8.63)	3.34	3.95	0.97	0.94
Ventromedial prefrontal cortex	46.78 (8.08)	48.09 (7.58)	3.94	4.47	0.95	0.92
Superior parietal cortex	47.34 (9.07)	48.40 (7.98)	6.19	6.82	0.90	0.85
Anterior cingulum	47.90 (8.17)	48.73 (7.06)	4.05	4.62	0.94	0.91
Posterior cingulum	55.86 (10.55)	57.59 (10.27)	3.94	3.61	0.96	0.96
Insula	45.09 (8.09)	45.34 (6.59)	5.81	5.82	0.91	0.85
Ventral striatum	37.66 (6.91)	38.83 (7.11)	4.89	4.18	0.93	0.95
Thalamus	42.64 (8.42)	43.58 (8.30)	7.17	4.30	0.88	0.95

Region of interest	Mean CBF(SD)		wsCV [%]		ICC	
	Ses 1	Ses 2	Ses 1	Ses 2	Ses 1	Ses 2
Hippocampus	37.90 (6.81)	38.21 (6.34)	4.88	4.64	0.93	0.93
Amygdala	36.51 (6.91)	36.73 (5.92)	5.49	6.55	0.92	0.86

Table 3

Evaluation of CBF (mean, wsCV and ICC) across task conditions in the regions of interest (ROI).

Region of interest	Mean CBF(SD)				wsCV [%]				ICC			
	FIX	EO	EC	PVT	FIX	EO	EC	PVT	FIX	EO	EC	PVT
Gray matter	46.59 (7.16)	47.07 (7.76)	48.56 (8.06)	46.79 (7.56)	9.47	7.62	6.83	7.63	0.70	0.83	0.87	0.83
White matter	29.55 (5.02)	29.84 (5.34)	30.69 (5.45)	29.63 (5.18)	9.43	7.52	6.47	8.15	0.76	0.86	0.91	0.84
Frontal lobe	50.53 (7.79)	51.01 (8.33)	52.30 (8.54)	50.72 (7.99)	9.14	7.45	6.62	7.24	0.73	0.83	0.88	0.83
Temporal lobe	44.71 (6.87)	45.23 (7.66)	47.02 (7.96)	44.64 (7.41)	9.84	7.46	7.34	7.33	0.68	0.84	0.85	0.85
Parietal lobe	51.04 (7.94)	51.55 (8.51)	52.89 (8.78)	51.22 (8.25)	9.07	7.73	7.02	7.63	0.74	0.82	0.87	0.83
Occipital lobe	47.88 (8.19)	48.66 (8.89)	50.92 (9.77)	48.27 (8.64)	11.14	9.64	8.35	9.23	0.66	0.76	0.85	0.79
ACA territory	48.02 (7.43)	48.58 (8.00)	49.81 (8.29)	48.04 (7.79)	9.62	7.84	6.84	7.83	0.70	0.82	0.87	0.82
MCA territory	49.61 (7.62)	50.08 (8.26)	51.66 (8.50)	49.75 (7.91)	9.13	7.39	6.75	7.06	0.73	0.84	0.87	0.84
PCA territory	44.32 (7.46)	44.97 (8.14)	47.16 (8.90)	44.70 (8.02)	11.27	9.56	8.29	9.13	0.64	0.76	0.85	0.80
Dorsolateral prefrontal cortex	52.88 (8.54)	53.32 (9.00)	54.51 (9.00)	53.15 (8.71)	8.85	7.57	6.72	7.31	0.77	0.84	0.88	0.84
Ventromedial prefrontal cortex	46.80 (7.21)	47.75 (7.81)	48.71 (8.07)	46.47 (7.23)	10.30	7.19	6.98	7.44	0.67	0.85	0.86	0.82
Superior parietal cortex	46.70 (7.32)	48.28 (8.82)	50.08 (9.21)	46.41 (7.79)	11.30	9.68	8.12	8.73	0.62	0.77	0.85	0.79
Anterior cingulum	47.72 (7.17)	48.26 (7.72)	49.52 (7.58)	47.75 (7.04)	9.59	8.09	6.48	7.51	0.69	0.79	0.86	0.81
Posterior cingulum	56.62 (10.01)	56.74 (10.34)	56.95 (9.92)	56.59 (10.01)	9.30	8.51	7.97	9.34	0.77	0.83	0.83	0.79
Insula	44.44 (6.82)	44.72 (7.44)	46.66 (7.64)	45.04 (6.93)	9.82	8.93	7.18	7.87	0.68	0.75	0.84	0.80
Ventral striatum	37.77 (6.55)	38.41 (6.93)	38.99 (7.00)	37.81 (6.63)	11.59	8.12	7.86	7.82	0.65	0.82	0.84	0.84
Thalamus	42.86 (7.66)	42.55 (7.83)	43.21 (8.29)	43.82 (8.39)	11.85	10.20	8.55	9.92	0.63	0.71	0.82	0.78
Hippocampus	37.64 (5.91)	37.87 (6.29)	39.23 (6.80)	37.49 (6.34)	9.92	8.01	7.58	7.74	0.67	0.79	0.83	0.82
Amygdala	36.07 (5.97)	36.36 (6.26)	38.17 (6.76)	35.88 (6.00)	10.53	8.82	8.13	8.16	0.68	0.78	0.82	0.81